Rapid Communications

X-ray heating and electron temperature of laboratory photoionized plasmas

R. C. Mancini,[1] T. E. Lockard,[1] D. C. Mayes,[1] I. M. Hall,[1] G. P. Loisel,[2] J. E. Bailey,[2] G. A. Rochau,[2] J. Abdallah, Jr.,[3] I. E. Golovkin,[4] and D. Liedahl[5]

[1]*Department of Physics, University of Nevada, Reno, Nevada 89557, USA*
[2]*Sandia National Laboratories, Albuquerque, New Mexico 87185, USA*
[3]*Los Alamos National Laboratory, Los Alamos, New Mexico 87544, USA*
[4]*Prism Computational Sciences, Madison, Wisconsin 53711, USA*
[5]*Lawrence Livermore National Laboratory, Livermore, California 94550, USA*

(Received 1 April 2019; revised manuscript received 17 February 2020; accepted 13 April 2020; published 18 May 2020)

We discuss the experimental and modeling results for the x-ray heating and temperature of laboratory photoionized plasmas. A method is used to extract the electron temperature based on the analysis of transmission spectroscopy data that is independent of atomic kinetics modeling. The results emphasized the critical role of x-ray heating and radiation cooling in determining the energy balance of the plasma. They also demonstrated the dramatic impact of photoexcitation on excited-state populations, line emissivity, and radiation cooling. Modeling calculations performed with astrophysical codes significantly overestimated the measured temperature.

DOI: 10.1103/PhysRevE.101.051201

Photoionized plasmas are widespread in space and found in many astrophysical systems including ionized absorbers in active galactic nuclei, x-ray binaries, and the accretion disks surrounding black holes [1]. These plasmas are driven by photoexcitation and photoionization due to an x-ray flux characterized by a broadband distribution of photons. Yet, in spite of their relevance to astrophysics, the increasing number of observations from orbiting telescopes, and the complexity of the astrophysical environment, only a small number of laboratory experiments have been done using large-scale pulsed-power and laser facilities, in order to test modeling codes and establish what physics models are needed to describe these plasmas [2]. The photoionized plasma experiments performed so far have been used to discuss charge state distribution and analysis of spectroscopy observations [3–13]. Here, we focus on x-ray heating, radiative cooling, photoelectron thermalization, and electron temperature; these are central issues of photoionized plasmas. Once photoelectrons are produced they thermalize via electron-electron elastic scattering while also undergoing inelastic atomic processes with ions. Hence, the resulting electron temperature depends on x-ray flux and atomic physics. The question is then, for a given x-ray flux, plasma element, and atom number density, what is the electron temperature of the photoionized plasma? We address this fundamental question with experiments and Boltzmann kinetic and radiation-hydrodynamics modeling.

The setup of the gas cell experiment at the Z pulsed-power facility [14] comprised a cm-scale gas cell filled with neon at pressures $P = 7.5$, 15, and 30 Torr. The gas cell was positioned outside the return current canister with a front window at 4.3 cm from the z-pinch axis, and front and rear windows were sealed with 1.4-μm-thick Mylar [3,4]. The run-in phase of the tungsten wire-array plasma lasts for 100 ns, after which the plasma collapses on axis producing a broadband 200-TW burst of x rays with a photon-energy integrated flux at the front window of 1.3×10^{12} W/cm^2. Photoionized plasmas in astrophysics are characterized by the ionization parameter ξ defined as the ratio of x-ray flux over the particle number density [15]. Values of $\xi \gg 1$ erg cm/s are relevant for astrophysics. By changing the distance to the z-pinch source and/or filling pressure, gas cell experiments provide a range of ξ of up to 60 erg cm/s. Since reradiation from hardware surrounding the z pinch is important, the x-ray flux photon-energy distribution is non-Planckian and cannot be well approximated by a geometrically diluted Planckian, but rather by a linear combination of three scaled Planckians. The most energetic one can be interpreted as due to the contribution of the z pinch while the other two represent the effect of hardware reradiation. At the peak of the x-ray drive, the maximum of the distribution is located at $h\nu_{\max} = 179$ eV and thus characteristic of a color (i.e., spectral) temperature $T_C = 62$ eV. The photon-energy integrated brightness temperature is $T_B = 60$ eV (see Fig. 1). The ionization potentials of neon from the neutral atom to the Li-like ion fall in the energy range from 20 to 240 eV, well within the bulk of the distribution. However, for He-like neon, $I_P = 1195$ eV, an energy located in the tail of the distribution; hence, only a small amount of H-like neon is populated.

The x-ray flux is employed in two different ways. On one hand, it ionizes the neon gas, turning it into a plasma with an atom number density in the range of 10^{17}–10^{18} cm^{-3}, depending on fill pressure, and an electron number density ~8 times larger. On the other hand, we record the transmission of a relatively narrow band in the photon energy range from 850 to 1250 eV with a spectrometer equipped with two elliptically bent potassium acid phthalate (KAP) crystals [16] capable of making simultaneous measurements with a spectral resolving power of $\lambda/\Delta\lambda \approx 1000$. Figure 2 displays a sample of the transmission spectrum. It shows absorption K-shell line transitions in Be-, Li-, He-, and H-like neon ions, indicating

 ©2020 American Physical Society

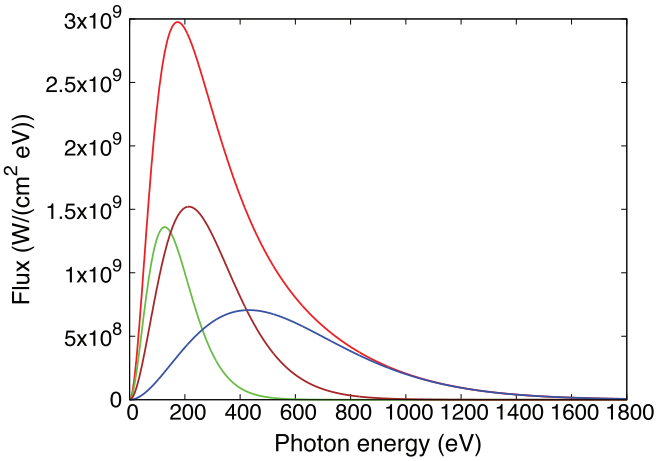

FIG. 1. Spectrally resolved x-ray flux impinging on the gas cell at the peak of the drive (red), and breakdown in three scaled Planckians of $T_R = 153$ eV (blue), $T_R = 76$ eV (brown), and $T_R = 45$ eV (green).

that a highly charged neon plasma has been produced. The analysis of the transmission spectrum permits the extraction of the areal densities of the absorbing ions within a time window of 3 ns around the peak of the x-ray drive.

The absorption lines in He- and H-like neon ions shown in Fig. 2 connect the ground with singly excited atomic states, while those in Be- and Li-like ions link ground and low excited states with autoionizing states with a vacancy in $n = 1$. In particular, the Li-like lines arise from states in the $1s^2 2s$ and $1s^2 2p$ configurations. The energy difference between these configurations is 16.2 eV. For the electron densities of these laboratory photoionized plasmas the relative population among these nearby configurations is dominated by electron collisions, i.e., electron collisional excitation dominates photoexcitation and electron collisional deexcitation dominates spontaneous and stimulated radiative decay. This fact is supported by a comparison of atomic

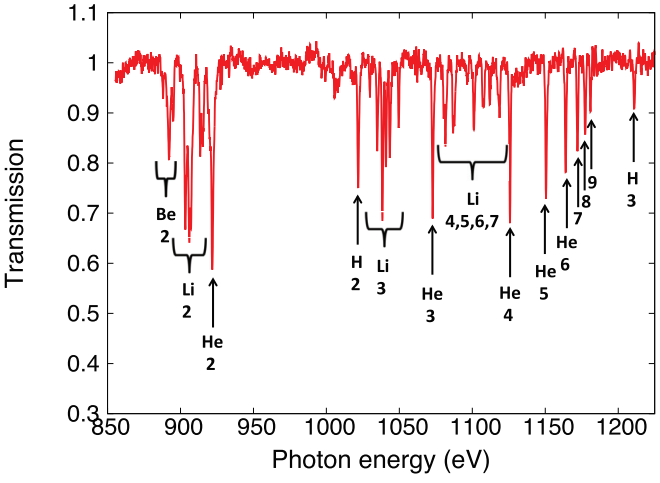

FIG. 2. Transmission data from Z shot z2222 ($P = 30$ Torr) showing K-shell line absorption in Be-, Li-, He-, and H-like neon ions. The labels indicate the neon ion and the upper (final) principal quantum number of the absorption transitions.

rates. More importantly, multi-ion and multi-energy-level collisional-radiative atomic kinetics calculations where these energy levels were connected by excitation-deexcitation and ionization-recombination processes to other energy levels in Be-, Li-, and He-like ions showed that this population ratio remains close to the Boltzmann value. Thus, for the conditions of our experiments, i.e., neon fill pressure and x-ray flux, we find that the relative populations of these two energy levels are close to equilibrium [local thermodynamic equilibrium (LTE)] while the overall charge state distribution is not in equilibrium [non-LTE (NLTE)]. This finding motivates the idea of extracting the electron temperature T_e of the photoionized plasma by interpreting the $1s^2 2p$ to $1s^2 2s$ population ratio with a Boltzmann factor. The idea is practical when kT_e (k is the Boltzmann constant) is comparable to the energy difference between levels ΔE. This method was tested first with the analysis of synthetic data; the extracted T_e was within 14% of the correct value. Next, the method was applied to the analysis of data from eight gas cell experiments performed over five series of Z shots. The results were $kT_e = 24^{+4}_{-6}$ eV for $P = 7.5$ Torr, $kT_e = 24^{+4}_{-5}$ eV for $P = 15$ Torr, and $kT_e = 26 \pm 5$ eV for $P = 30$ Torr. The uncertainties include data statistics and the approximation of interpreting the Li-like ion population ratio with a Boltzmann factor.

The question arises as to whether or not the plasma electrons are in thermal equilibrium. It is important to address this question for two reasons: first, to interpret the T_e extracted from data analysis; and second, to justify the use of a radiation-hydrodynamics model to simulate the experiment. We have addressed this question by using a time-dependent kinetics model that solves the Boltzmann equation for the electron distribution function simultaneously and self-consistently with a set of collisional-radiative kinetics rate equations for the ion's atomic level population distribution [17]. Both electron-electron elastic scattering and electron-ion inelastic atomic processes were considered. The rates of atomic processes involving free electrons were calculated using the distribution function determined by the Boltzmann equation, and the inelastic terms in the Boltzmann equation were calculated with the level populations from the atomic kinetics rate equations. Hence, driven by the x-ray flux, electron and atomic kinetics were intertwined and evolved self-consistently. The results indicated that the electrons thermalized quickly and the vast majority (over 99%) evolved through a series of equilibrium states that were well described by a single Maxwellian distribution. The high-energy tail of the distribution included only a small fraction of electrons with a characteristic temperature of a few hundred eV. Thus, for the conditions of the experiment, nonequilibrium effects in the electron distribution function occur on subnanosecond timescales and the temperature extracted from absorption spectroscopy can be interpreted as the electron temperature T_e of the plasma. This result was also consistent with estimates based on Spitzer's electron-electron equilibration times [18] that were under 110 ps.

The experiment was simulated with the one-dimensional radiation-hydrodynamics code HELIOS-CR [19], including front and rear windows and neon gas. Electrons and ions were allowed to have different temperatures T_e and T_i, respectively,

and their temperature equations were coupled by an electron-ion equilibration term. The simulations were driven by the time history of the photon-energy resolved x-ray flux incident on the front window. Detailed atomic physics and multiangle photon-energy resolved radiation transport were employed throughout the target. The photon-energy dependent emissivity and opacity of Mylar windows were modeled with atomic level populations calculated with equilibrium (LTE) atomic kinetics. However, for the neon atomic physics we used time-dependent collisional-radiative atomic kinetics (NLTE). The NLTE atomic kinetics was solved simultaneously and self-consistently with the radiation transport equation, and calculated inline with the hydrodynamics. The input x-ray flux was attenuated by the front window; at the time of the drive peak, 75% of x-ray energy was being transmitted. The expansion of front and rear windows launched two shocks into the neon so that the hydrodynamically unperturbed (motionless) photoionized neon plasma was located in between two narrow layers of shocked neon. The simulation showed that the unshocked neon plasma was nearly spatially uniform. To check the T_e extraction method, we calculated the time history of the emergent x-ray intensity distribution from the rear window by transporting the radiation through the entire system using the complete temperature and density spatial profiles. The results confirmed that plasma self-emission in the photon energy range of the Li-like lines was negligible compared to the backlighter intensity, the formation of the Li-like line absorption spectrum was dominated by transmission through the photoionized plasma, and the spectrum analysis gave the photoionized neon plasma T_e.

In the HELIOS-CR simulation, spatial gradients and fluid motion are negligible in the photoionized neon plasma region. Hence, the T_e equation can be approximated by

$$C_{V,e}\frac{dT_e}{dt} \approx -\omega_{ei}(T_e - T_i) + R_H - R_C, \qquad (1)$$

where $C_{V,e}$ is the electron specific heat, and ω_{ei} is the thermal electron-ion coupling coefficient (inversely proportional to the electron-ion equilibration time). The radiation heating R_H and cooling R_C rates are given in terms of integrals over the photon energy of the opacity times the radiation field energy density (for R_H) and of the emissivity (for R_C) [20]. Figure 3 shows the time histories of R_H, R_C, and the net heating rate $R_N = R_H - R_C$ of the photoionized neon plasma from the simulation of a gas cell with $P = 30$ Torr (10^{18} cm^{-3}). A positive R_N indicates that the plasma is being radiatively heated, i.e., that it is absorbing more radiation energy than it is losing by emission. We note that the maxima of the radiation rates occurs at 96.8 ns, when the population of Li-like neon is the largest and before the peak of the x-ray drive at $t = 100$ ns. This is an indication that the x-ray heating depends on both the strength of the x-ray drive and the state of the plasma. As ionization burns through Li-like neon ($I_P = 239$ eV), it begins to populate the $1s^2$ closed shell of He-like neon ($I_P = 1195$ eV). This is reflected in a significant decrease in opacity between photon energies $h\nu = 70$ eV and $h\nu = 800$ eV where the bulk of the drive photons are located. Further ionization beyond the He-like ground state requires photons in an energy range where the drive is weak. Hence, plasma heating and ionization diminish substantially.

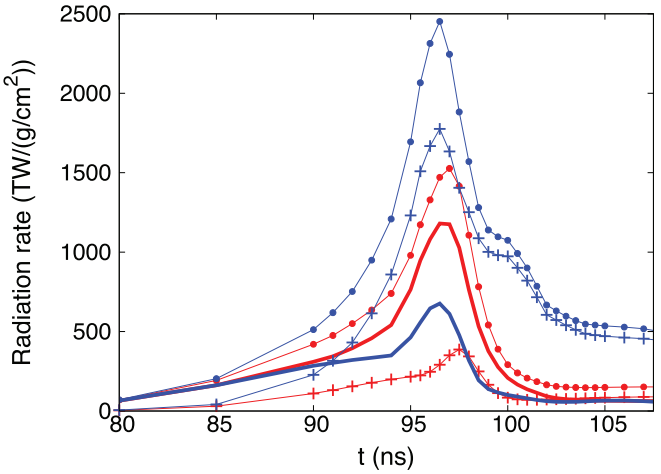

FIG. 3. Time histories of radiation heating R_H (•), cooling R_C (+), and net heating $R_N = R_H - R_C$ (thick lines) rates from the HELIOS-CR simulation of the neon gas cell experiment for $P = 30$ Torr. Results are shown including full (blue) and scaled-down (red) photoexcitation rates. The peak of the x-ray drive is at $t = 100$ ns.

Photoexcitation driven by the broadband x-ray flux populates excited states that, in turn, are critical for determining the line emission contribution to plasma emissivity and radiation cooling. Since electrons in photoionized plasmas have relatively low temperatures, photoexcitation is a key mechanism to populate excited states. Electrons further contribute by redistributing population among nearby energy levels and via three-body recombination. Photoexcitation followed by photoionization or autoionization from excited states impacts the plasma charge state distribution as well. To illustrate the importance of photoexcitation on plasma heating, Fig. 3 also shows simulation results for $P = 30$ Torr where photoexcitation (and stimulated emission) rates scaled down by 10^{-3} were used in the level population calculation *only*, i.e., once the level populations were computed, R_H and R_C were calculated with full rates. The point of this calculation was to assess the effect of photoexcitation on atomic level populations. The change in level populations affects both plasma emissivity and opacity. However, the impact on emissivity is larger than that on opacity since line contributions to the emissivity depend on excited-state populations while to the opacity on ground and low excited states. For $P = 30$ Torr, this is reflected in a dramatic overall reduction of R_C. The peak value of R_C was reduced by a factor of 4.6 while that of R_H by 1.6, and R_N was increased by 1.8. For $P =$ 7.5 and 15 Torr the changes were qualitatively similar but larger in value, indicating that the effect is stronger at lower densities.

Figure 4 displays T_e measurements and time histories from HELIOS-CR simulations performed for $P = 7.5$, 15, and 30 Torr; averaged kT_e values during the time interval of the measurement are 23, 24, and 26 eV, respectively. These values compare well with the observations. HELIOS-CR simulations with scaled-down photoexcitation rates resulted in larger R_N (see Fig. 3), as well as larger averaged kT_e: 63, 60, and 57 eV for $P = 7.5$, 15, and 30 Torr, respectively. Figure 4 also shows the T_e computed by Boltzmann kinetics for $P = 7.5$ and

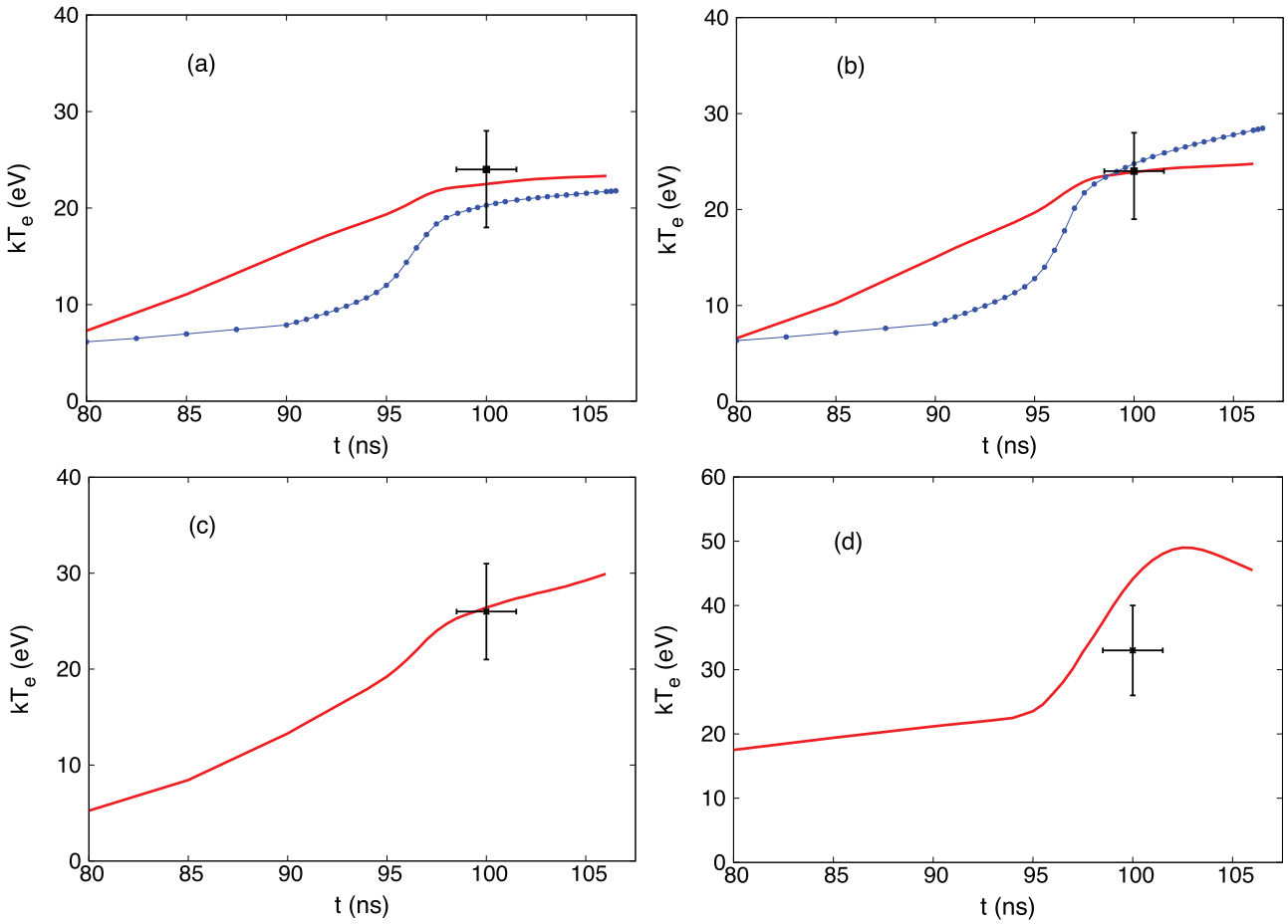

FIG. 4. Electron temperature measurements and time histories from HELIOS-CR simulations of neon gas cell experiments (red lines) for (a) $P = 7.5$, (b) 15, and (c) 30 Torr, and from Boltzmann kinetics (blue lines with dots) for $P = 7.5$ and 15 Torr. The measurement and HELIOS-CR simulation of the SiO-tamped foil experiment are also shown (d). The peak of the x-ray drive is at $t = 100 \pm 0.5$ ns.

15 Torr, which had averaged $kT_e = 20$ and 25 eV, respectively. This fundamental kinetic approach to model heating is also an independent and complementary calculation of T_e. It models heating by tracking the evolution of the electron distribution function while free electrons gain or lose energy to inelastic atomic processes. Radiation hydrodynamics and Boltzmann T_e results are comparable in the time interval of the measurement. However, since the Boltzmann model is optically thin it overestimates radiation cooling, which results in lower T_e at earlier times.

It is particularly interesting to compare with codes used to model photoionized plasmas in astrophysics. We considered CLOUDY [21] and XSTAR [22]. These codes solve an energy balance equation self-consistently with a set of collisional-radiative atomic kinetics equations and the radiation transport equation. Since the codes assume a steady state, we applied them to $P = 30$ Torr in order to minimize residual transient effects. Both models overestimated T_e at the x-ray drive peak, $kT_e = 55$ and 65 eV, given by CLOUDY and XSTAR, respectively.

The same Li-like ion population ratio method for extracting T_e was tested and applied to a different photoionized plasma experiment performed at Z and discussed elsewhere [13]. In this case, a plastic-tamped silicon-oxygen thin slab underwent a controlled expansion driven by the Z x-ray flux to produce a photoionized plasma that, at peak x-ray flux, had a number density comparable to that of the neon gas cell experiment with $P = 30$ Torr, i.e., 10^{18} cm^{-3}. The relative atomic concentration Si/O was 2. Different from the neon plasma that is dominated by K-shell ions, now B-, Be-, and Li-like L-shell ions dominate the silicon charge state distribution. The silicon K-shell line absorption spectrum was recorded to diagnose the plasma. In particular, the Li-like silicon $1s^2 2p/1s^2 2s$ population ratio was also found to be useful to extract T_e. In this experiment we obtained $kT_e = 33 \pm 7$ eV. The HELIOS-CR radiation-hydrodynamics simulation of the experiment with inline NLTE silicon and oxygen atomic physics produced an averaged $kT_e = 43$ eV, just above the range of the measurement (see Fig. 4). Again, the simulation with scaled-down photoexcitation rates resulted in reduced R_C and R_H (R_C more than R_H), and a significant increase in R_N (see Fig. 5). At the peak of the drive ($t = 100$ ns), R_C and R_H were reduced by factors of 2.7 and 1.5, respectively, while R_N was increased by a factor of 2.3. These changes produced a larger averaged $kT_e = 95$ eV. This result confirmed the same dramatic effect found for the neon plasma but now in a photoionized silicon plasma dominated by L-shell ions. Also, modeling calculations done with CLOUDY and XSTAR for peak drive conditions overestimated heating and produced $kT_e = 73$ and 69 eV, respectively.

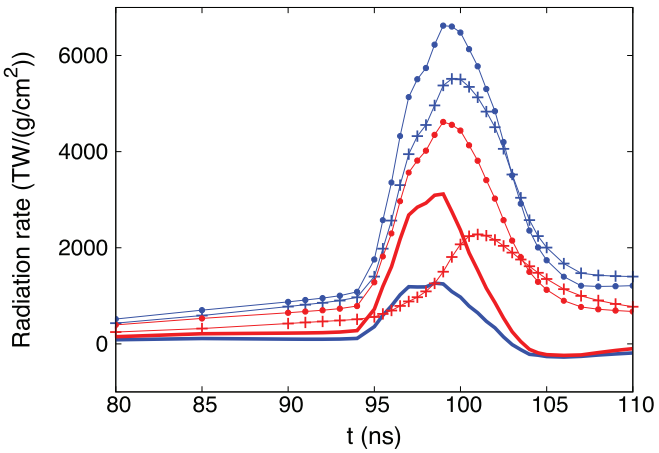

FIG. 5. Time histories of radiation heating R_H (•), cooling R_C (+), and net heating $R_N = R_H - R_C$ (thick lines) rates from the HELIOS-CR simulation of the SiO expanding foil experiment. Results are shown including full (blue) and scaled-down (red) photoexcitation rates. The peak of the x-ray drive is at $t = 100$ ns.

In photoionized plasmas x-ray photons interact with ions through photoexcitation and photoionization. This leads to a key interplay between atomic physics and heating. We note in passing that this is different from laser-produced plasmas where optical photons interact with plasma electrons that, in turn, drive ionization and atomic kinetics. Modeling calculations showed the critical effect of photoexcitation on R_C. This effect was independently confirmed with standalone, steady-state collisional-radiative atomic kinetics calculations. In the Z experiments, it was found to be important in both neon and silicon plasmas. The former is an example of a plasma dominated by K-shell ions while the latter by L-shell ions, i.e., different plasma elements and atomic physics but the same finding. Moreover, a systematic analysis of the impact of collisional ionization-recombination and excitation-deexcitation, and radiative and dielectronic recombinations produced much smaller changes on R_C than the changes due to photoexcitation.

This Rapid Communication has addressed the fundamental problem of heating and temperature in laboratory photoionized plasmas with experiment and modeling. The Boltzmann kinetics approach for modeling photoelectron thermalization is promising, particularly as future experiments will consider lower densities. Although the electron distribution function was found to be largely Maxwellian, Boltzmann kinetics also provided unique information about the high-energy tail of the distribution. Along with photoexcitation, these energetic electrons can be important for the analysis of line emission spectra from photoionized plasmas.

Explaining the T_e overestimation produced by CLOUDY and XSTAR in the Z experiments is important and will be the object of future research. We note that the application of photoionization modeling calculations done with XSTAR to interpret the Cygnus X-3 x-ray spectrum recorded with Chandra produced a significant overestimation of the T_e measured from the analysis of radiative recombination emission [23]. The multielement nature of the Cygnus X-3 plasma and the complexity of the astrophysical scenario make modeling of the Chandra observation challenging. Yet, this Rapid Communication shows that XSTAR and CLOUDY have problems modeling the energy balance of neon as well as silicon photoionized plasmas in controlled and reproducible laboratory experiments.

The modeling of radiation cooling in CLOUDY is discussed in Ref. [24]. The effort to include the best-quality atomic physics databases is remarkable. However, it may come at the expense of working with an inconsistent set of atomic data and/or an incomplete description of the energy-level structure. Both points have been found to be important in atomic physics models applied to laboratory data [25]. Whether this or some other reason explains the T_e overestimation, the Z experiments present an opportunity to revise and improve astrophysical codes, especially the evaluation of atomic excited-state populations and line emissivity and its effect on radiation cooling and heating. Such a revision would impact and increase confidence in their astrophysical applications as well.

This work was supported in part by DOE OFES Grant No. DE-SC0014451, DOE NNSA Grant No. DE-NA0003875, the Z Fundamental Science Program, and the Wootton Center for Astrophysical Plasma Properties. Sandia National Laboratories is a multimission laboratory managed and operated by National Technology and Engineering Solutions of Sandia, LLC, a wholly owned subsidiary of Honeywell International, Inc., for the US Department of Energy's National Nuclear Security Administration under Contract No. DE-NA-0003525. This paper describes objective technical results and analysis. Any subjective views or opinions that might be expressed in the paper do not necessarily represent the views of the US Department of Energy or the US Government. Lawrence Livermore National Laboratory is operated by Lawrence Livermore National Security, LLC, for the US Department of Energy, National Nuclear Security Administration under Contract No. DE-AC52-07NA27344.

[1] D. E. Osterbrook and G. J. Ferland, *Astrophysics of Gaseous Nebulae and Active Galactic Nuclei* (University Science Books, Mill Valley, CA, 2006).

[2] R. C. Mancini, J. E. Bailey, J. F. Hawley, T. Kallman, M. Witthoeft, S. J. Rose, and H. Takabe, Phys. Plasmas **16**, 041001 (2009).

[3] J. E. Bailey *et al.*, J. Quant. Spectrosc. Radiat. Transfer **71**, 157 (2001).

[4] I. M. Hall, T. Durmaz, R. C. Mancini, J. E. Bailey, G. A. Rochau, I. E. Golovkin, and J. J. MacFarlane, Phys. Plasmas **21**, 031203 (2014).

[5] M. E. Foord, R. F. Heeter, P. A. M. van Hoof, R. S. Thoe, H. K. Chung, D. A. Liedahl, P. T. Springer, J. E. Bailey, M. E. Cuneo, G. A. Chandler, L. P. Mix, C. Ramsbottom, R. Kisielius, V. Jonauskas, F. P. Keenan, S. J. Rose, and W. H. Goldstein, Phys. Rev. Lett. **93**, 055002 (2004).

[6] S. J. Rose, P. A. M. van Hoof, V. Jonauskas, F. P. Keenan, R. Kisielius, C. Ramsbottom, M. E. Foord, R. F. Heeter, and P. T. Springer, J. Phys. B **37**, L337 (2004).
[7] M. E. Foord *et al.*, J. Quant. Spectrosc. Radiat. Transfer **99**, 712 (2006).
[8] F.-L. Wang, S. Fujioka, H. Nishimura, D. Kato, Y.-T. Li, G. Zhao, J. Zhang, and H. Takabe, Phys. Plasmas **15**, 073108 (2008).
[9] S. Fujioka *et al.*, Nat. Phys. **5**, 821 (2009).
[10] F.-L. Wang, D. Salzmann, G. Zhao, H. Takabe, S. Fujioka, N. Yamamoto, H. Nishimura, and J. Zhang, Astrophys. J. **706**, 592 (2009).
[11] E. Hill and S. J. Rose, Phys. Plasmas **17**, 103301 (2010).
[12] Z. Wu, B. Duan, Y. Li, and J. Yan, High Energy Density Phys. **23**, 153 (2017).
[13] G. P. Loisel, J. E. Bailey, D. A. Liedahl, C. J. Fontes, T. R. Kallman, T. Nagayama, S. B. Hansen, G. A. Rochau, R. C. Mancini, and R. W. Lee, Phys. Rev. Lett. **119**, 075001 (2017).
[14] J. E. Bailey *et al.*, Phys. Plasmas **9**, 2186 (2002).
[15] C. B. Tarter and E. E. Salpeter, Astrophys. J. **156**, 953 (1969).
[16] P. W. Lake, J. E. Bailey, G. A. Rochau, P. Gard, D. Petmecky, M. Bump, N. R. Joseph, T. C. Moore, and L. B. Nielsen-Weber, Rev. Sci. Instrum. **77**, 10F315 (2006).
[17] J. Abdallah, Jr. and J. Colgan, J. Phys. B **45**, 035701 (2012).
[18] L. Spitzer, Jr., *Physics of Fully Ionized Gases* (Wiley, New York, 1962).
[19] J. J. MacFarlane, I. E. Golovkin, and P. R. Woodruff, J. Quant. Spectrosc. Radiat. Transfer **99**, 381 (2006).
[20] D. Mihalas, *Stellar Atmospheres* (W. H. Freeman, New York, 1978).
[21] G. J. Ferland, K. T. Korista, D. A. Verner, J. W. Ferguson, J. B. Kingdon, and E. M. Verner, Publ. Astron. Soc. Pac. **110**, 761 (1998).
[22] T. Kallman and M. Bautista, Astrophys. J., Suppl. Ser. **133**, 221 (2001).
[23] T. Kallman *et al.*, Astrophys. J. **874**, 51 (2019).
[24] M. L. Lykins, G. J. Ferlamd, R. L. Porter, P. A. M. van Hoof, R. J. R. Williams, and O. Gnat, Mon. Not. R. Astron. Soc. **429**, 3133 (2013).
[25] S. B. Hansen, Balancing detail and completeness in collisional-radiative models, in *Modern Methods in Collisional-Radiative Modeling of Plasmas*, edited by Y. Ralchenko, Springer Series on Atomic, Optical and Plasma Physics Vol. 90 (Springer, Berlin, 2016), Chap. 1.